Renewable Energy 216 (2023) 119063

Contents lists available at ScienceDirect

Renewable Energy

journal homepage: www.elsevier.com/locate/renene

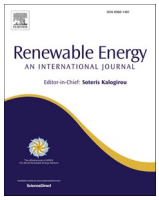

Controller design for a tidal turbine array, considering both power and loads aspects

Yidan Zhang *, Jonathan K.H. Shek, Markus A. Mueller

Institute for Energy Systems, School of Engineering, The University of Edinburgh, Faraday Building, Edinburgh, EH9 3DW, UK

ARTICLE INFO

Keywords:
Tidal current turbine
Tidal turbine array control
Axial induction factor control
Active wake control

ABSTRACT

The complex turbine-wake interactions within a tidal array leads to sub-optimal power generation from most tidal turbines, and results in higher fatigue loading on downstream turbines due to upstream turbines increase the turbulence intensity in the wake reaching other turbines. This paper presents an array controller which determines the power and loads set-points between the turbines based on incoming flow velocity for each turbine. This control methodology enables to dynamic response in time-variable flow velocity and trade-off between output power and fatigue loads through adjusting reference pitch angle and maximum power point tracking reference speed simultaneously for each turbine. The benefits of this novel control strategy is tested in a 4.5 MW three-turbine array model which is simulated in MATLAB/Simulink. Results show that in low flow velocity, the objective of stabilizing the fluctuation of loads is mainly achieved by adjusting generator speed. Conversely, the pitch controller dominates the results of the array in high flow velocity. Under the premise of mitigating fatigue loads, the proposed control strategy is still able to guarantee a high-level output power extraction.

1. Introduction

Tidal currents are a potential renewable energy source with broader perspectives due to high predictability and stability. This means that tidal energy provides the energy buffer in a system that will increasingly depend on distributed energy; grid operators are able to plan for the amount of tidal energy extraction, and schedule other sources to fill the gap in order to improve energy security.

The tidal current devices, which utilize these currents, are broadly similar to wind turbines and are used to convert ocean current into kinetic energy through rotor rotating. Since water is roughly 830 times denser than air, tidal current can generate more energy per unit area than winds. Therefore, another benefit of tidal power is the relatively small footprint of tidal turbines, compared to wind turbines, which enable high energy density compact arrays. Recent research suggests average power densities of tidal arrays in the 35–50 MW/km^2 range, which is much higher than the 4–7 MW/km^2 seen on average for offshore wind farms [1–3]. Moreover, it is less visually impacting than offshore wind power as turbines are completely submerged. Due to similarities in the drive train, tidal energy developers can take advantage of the experience from more advanced and mature science and engineering techniques gained from the wind energy industry, including design, manufacture, operation and maintenance, thereby accelerating the development of tidal current conversion technologies and rapidly move towards commercialization.

Horizontal axis tidal turbines (HATT) are the most technologically mature out of all the marine renewable energy devices currently under development, as full-scale prototypes are already being tested and operated. There have been a number of examples of the commercial maturity of HATTs; for instance, the world's first grid connected commercial tidal device - 1.2 MW SeaGen turbine incorporates twin 600 kW horizontal axis rotor which implemented in 2008 by Marine Current Turbines (MCT); it was successful decommissioned in 2019, having exported 11.6 GWh to the grid [4]. Following MCT's acquisition by Siemens, more advanced SeaGen-S 2 MW turbine is being developed and tested [5]. 1 MW HS 1000 and 1.5 MW HS 1500 are developed by Andritz Hydro Hammerfest; HS1000 is the first pre-commercial tidal current turbine (TCT) to validate the technology for the world's first tidal power array system at European Marine Energy Centre (EMEC), and it was connected to the grid in February 2012 [6]. SIMEC Atlantis Energy developed AR 1500 and AR 2000 turbines, which are rated at 1.5 MW and 2 MW respectively; AR 2000 is the world's largest single rotor tidal turbine [7]. A two-bladed rotor design (M100) was developed by Nova Innovation, and a subsequent revision, the M100-D, eliminated

* Corresponding author.
E-mail address: yidan.zhang@ed.ac.uk (Y. Zhang).

https://doi.org/10.1016/j.renene.2023.119063
Received 23 December 2022; Received in revised form 17 May 2023; Accepted 17 July 2023
Available online 20 July 2023
0960-1481/© 2023 The Authors. Published by Elsevier Ltd. This is an open access article under the CC BY license (http://creativecommons.org/licenses/by/4.0/).

the need for a gearbox that can improve the efficiency and drive down the cost [8]. All these devices are mounted on the seabed, while some HATT manufacturers like Orbital Marine Power and Magallanes Renovables are testing floating turbines that are moored to the seabed. Orbital's 2 MW O2 tidal turbine is able to meet the annual electricity demand for around 2000 homes [9].

However, large scale tidal energy production is still in its infancy; technology readiness and high costs are widely acknowledged by the industry as being critical reasons of hindering its expansion. The estimated operation and maintenance cost of ocean energy devices is about 60% higher compared with offshore wind [10]. A key challenge is that tidal devices operate in a hostile offshore environment where they need to withstand unsteady and large hydrodynamic loads. Therefore, the key economic issue, that the tidal energy industry, faces is how to reduce the high cost of construction, operation and maintenance, in order to reduce the levelized cost of energy (LCOE) [11].

To make tidal technology economically viable and competitive with other renewable energy sources, developers are trying to deploy hundreds of tidal current turbines (TCT) in an array in order to extract an economically useful amount of power; significant cost reduction can be achieved through spreading fixed project costs over a larger number of devices [12]. A key aspect of developing large scale power generation is determining how to control each single turbine to extract maximum averaged power over a tidal cycle to increase revenue. Also, a significant reduction of operation and maintenance (O&M) costs can be achieved by reducing unexpected maintenance and increasing the lifetime of critical components. Several pilot projects, multi-MW sized tidal turbine array, are operating in various parts of the world.

Some commercial demonstrator projects have tested in realistic tidal channels. The world first TCT array was developed by Nova Innovation at Bluemull Sound in Shetland; the first three Nova M100 devices with are total installed capacity of 300 kW were deployed in 2016 and 2017. Also, this tidal array is the first array to supply electricity to the grid with more than 17000 generating hours reached in 2019 [8]. In 2020, a fourth 100 kW turbine was added to the array. With the installation of a further two 100 kW turbines, it became the world's largest array (by turbine number) with a total of six turbines [13]. Another global developer of tidal current energy, SIMEC Atlantis Energy, developed the MeyGen project at the Pentland Firth in 2016. The array consists of four 1.5 MW turbines; one AR1500 turbine and three HS1500 turbines, with total capacity of 6 MW. This MeyGen array has been operational since 2017 and generated 50 GWh of electricity as of February 2023. This is more than double the total generation from tidal devices elsewhere in the world [14]. Expansion of the project is already underway. After the installation of a subsea hub in September 2020, there are plans to connect two additional AR2000 turbines via the new hub [15].

Until now, there is no consensus as to the best approach for the design and operation of tidal turbine arrays which includes the number of devices, layout, control strategy and electrical architecture. Normally, the strategy of extracting maximum power of each tidal turbine does not result in maximal power capture for the entire array. The reason is that the upstream turbines slow down the flow velocity that reaches downstream turbines, by extracting too much power [16,17]. This is due to complex turbine-wake interactions leading to sub-optimal power generation from most tidal turbines within the array.

Therefore, a controller should be designed for the array to adjust the power extraction to maximize average power, which will increase revenue. Design of controllers for TCT arrays presents a challenge to prognosticate the effect of the wake formed behind a tidal turbine on the other turbines. This challenge originates in a significant reduction in mean flow velocity reaching downstream turbines, and the increment in turbulence [18]. The tidal flow fluctuations experienced by downstream turbines are greater than upstream turbines and result in a substantial increase in fatigue loading [19]. It is for this purpose that an array controller should employ proper strategies to distribute the power set-points between the turbines to mitigate fatigue loads, so that O&M costs can be reduced. Both of these, power maximization and mitigation of fatigue loads, help to reduce LCOE.

To date, the research into TCT array optimization can be briefly divided into two main categories. The first is the arrangement of turbines; the layout of arrays can be classified into aligned arrays and staggered arrays. However, tidal array layout optimization techniques are typically limited by some geographical factors; since suitable sites for arrays often lie in concentrated energy flow along short and narrow tidal channels [20,21], the number of turbines that can be deployed is limited. According to a study from Vennell et al., expanding an array by deploying more turbines in the same cross-section across the channel can increase the power output of every turbine within the array, despite a reduction in flow within the channel [20,22,23]. An efficient gradient-based optimization algorithm for optimizing array layout rapidly in an infinite tidal channel is proposed in Ref. [24]. In this paper, results show that turbines should be located in one row as much as possible, which would increase the output power of a large-scale turbine array by 24%. According to an experimental study from Daly [25], an accelerated flow region can be found in a particular inter-turbine spacing layout that can be used for high power production. It was particularly noted that a flow acceleration of up to 14% can be achieved due to turbine arrangement.

A study of a staggered configuration of a tidal farm showed that small longitudinal spacing offers high efficiency [26]. The experimental work also suggests that a staggered configuration might be a better option for large-scale tidal current turbine arrays to reduce wake interaction and possibly higher power extraction from accelerated flow [27]. A three-dimensional numerical model, Telemac 3D, is used to investigate the flow interactions between turbines in the tidal site, Alderney Race. The results show that the output power of the staggered layout is 16% higher than the aligned layout [16].

The second category is the Active Wake Control (AWC) strategies, through individually tuning the turbines in an array (for a certain turbine array in a particular channel, the location of each turbine is already known). This control aims to reduce wake losses in an array in order to increase the energy yield and/or decrease loading. AWC methods can divided into two classes. The first class is the wake redirection control, which can be achieved through misaligning yaw angle. Yaw control redirects the turbine wakes by yawing or tilting of the turbines. However, due to limited dynamic response, the yawing mechanism typically does not change frequently to continuously align with time-variable tidal flow [28]. Also, the yaw system may impose an additional mechanical stress on the turbine [29]. The second class of AWC methods is called axial induction factor control and contains strategies which aim to reduce the wake deficit downstream by changing the axial induction factor of upstream turbines. This can be achieved down-regulating the upstream turbines, either by adjusting pitch angle and/or operating at a suboptimal tip-speed ratio (TSR). Altering these two parameters separately or simultaneously will change the power, torque and thrust coefficients of turbines and affect the generated power and loadings.

Vennell was the first to show that the turbine resistance needs to be tuned for a given channel and turbine arrangement in order to maximize the performance of a TCT array. Vennell provides key insights into the importance of tuning TCTs in an array, where three numerical tuning strategies are proposed to maximize the average output over the whole tidal cycle for one turbine in an array [30]. These strategies adjust the blockage ratio of each turbine to produce a higher output power, often without increasing the maximum loading on the turbines and whilst also maintaining a higher channel flow rate. However, array controller design for tidal turbines is still lacking, especially in utilizing the control of individual turbines to maximize the performance of the array as a whole; to achieve this, there is a need to determine the appropriate pitch angle and rotational speed of the turbine rotor for each turbine based on different incoming flow velocities.

Conversely, significant research into the axial induction factor based (AIF) control has been conducted in wind farms. An experimental study

proposed by Bartl and Saetan [31] investigated the effects of modifying TSR or blade pitch angle alone on total array efficiency of two in-line upwind turbines; a small increase on the whole array output was observed. Moreover, results demonstrated that axial induction factor control can potentially even out load distribution between two consecutive turbine rows. A wind farm control design which focuses on optimization of both power and load simultaneously has been proposed by Soleimanzadeh and Wisniewski [32], in order to maximize power and reduce fatigue loads. This control design only adjusts rotor speed in low wind speed, and only varies pitch angle in high wind speed. The results imply that fluctuations in the drive train torque, caused by variable wind, can be reduced by reducing the rotor speed or by pitching the blades. However, large variations in the pitch blade angle for upwind turbines seem to compromise the performance of the torque controller.

Therefore, for a tidal turbine array, the tuning of individual turbines needs to be carried out in coordination with torque control; the trade-off between blade pitch and torque control strategies must be considered. It is suggested in this paper a control methodology for a TCT array, which determines the power and loads set-points between the turbines based on incoming flow velocity for each turbine. Subsequently, pitch angle and TSR for each turbine can be adjusted simultaneously so that the requirements can be met for maximizing the whole array output averaged over the tidal cycle and also mitigate fatigue loads. The performance of this array control strategy is outlined with particular emphasis on the dynamic response in time-variable flow velocity and the trade-off between output power and fatigue loads. The application of an axial-induction-factor-based (AIF-based) TCT array controller in a full resource-to-grid model, whilst considering both loads and power has been done for the first time.

This paper begins with a brief introduction to the modelling and simulation of a TCT array in section II. Each turbine includes an individual detailed electromechanical turbine model developed in MATLAB/Simulink, from resource to the grid. In section III, a novel array control strategy that determines the optimal reference signals of pitch angle and tip speed ratio for each single turbine is described. Section IV presents and compares the system performance under conventional and axial induction factor control. Finally, conclusions are derived in section V.

2. Tidal current turbine array modelling and simulation

The TCT array model considers turbine array arrangement and the determination of downstream flow velocity under multiple wake effects. Also, a grid connection scheme for this turbine array will be described. This array was modelled based on a single tidal turbine model, rated at 1.5 MW, which refers to previous work done in Refs. [33,34]. This section starts with the introduction of modelling and simulation of an individual turbine. Fig. 1 shows the arrangement of the proposed TCT array and tidal current energy conversion system for a single turbine.

2.1. The tidal resource

Measurements of tidal site characteristics are direct driven by the requirements of tidal turbine developers. A comprehensive understanding of the dynamic of tidal currents is essential to improve device design, turbine array reliability and ultimately energy conversion rate. For the purpose of this study the input tidal current resource is represented by a half-cycle of a semidiurnal spring tide with high peak flow, as it is intended that the model should represent the most complex operational period of the system. The tidal flow velocity is constructed by mean flow velocity and predicted turbulence.

- The mean flow velocity, $\overline{V}$ was derived from actual tidal current measured data in the ReDAPT Project; Brian et al. used Acoustic Doppler Current Profilers (ADCP) to measure three-dimensional tidal flow velocities at the EMEC [35]. The tidal velocity measurements taken from Doppler devices were time averaged. In Fig. 2, the chosen half-cycle of the tidal current is shown.
- The predicted turbulence is modelled by adding band-limited white noise. The added turbulence was chosen to have intensity of 10% from the mean flow velocity. Tidal current velocity with added turbulence intensity is shown in Fig. 3. This flow velocity profile used as freestream flow, input to the array models.

2.2. Single turbine model

The permanent magnet synchronous generator (PMSG)-based tidal turbine system developed in MATLAB/Simulink is depicted in Fig. 1.

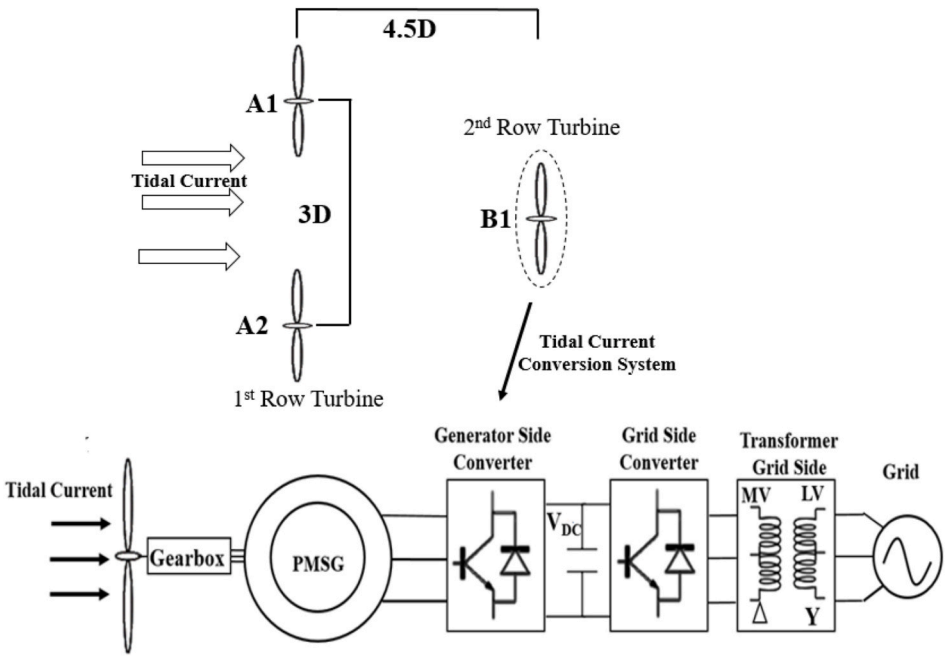

Fig. 1. The arrangement of TCT array and full resource-to-grid tidal current conversion system.

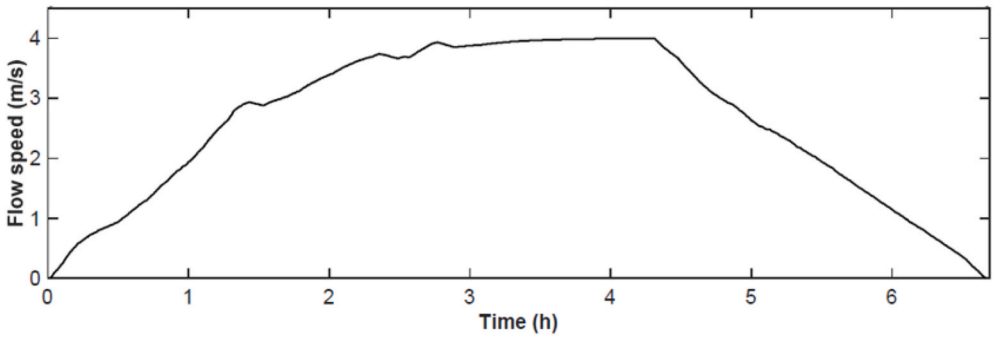

Fig. 2. The half-cycle of the mean tidal current velocity data.

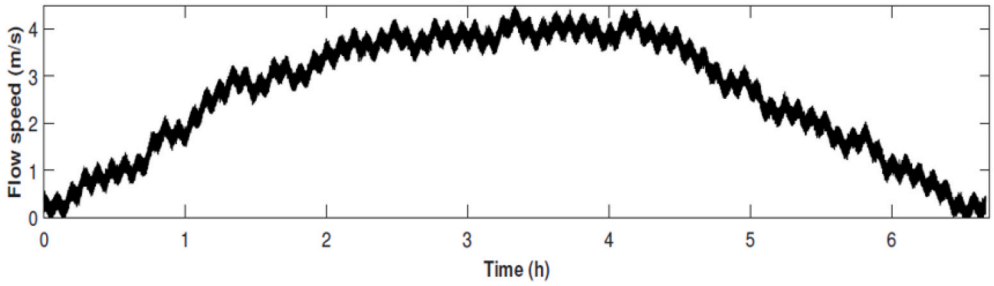

Fig. 3. Tidal current velocity with added turbulence intensity.

This full resource-to-grid model consists of the tidal current resource, the three-bladed and pitch-controlled turbine, and the generator which is controlled by an active rectifier and DC link. The inverter and transformer are used to deliver power to feed into the grid.

2.2.1. Hydrodynamics of the turbine

As the tide ebbs and flows, turbine blades are driven to rotate to extract mechanical power, P_{mec} from tidal current. The output of the turbine rotor is mechanical torque, T_{mec}, which is used as input to the generator; a shaft and a gearbox are required to deliver this T_{mec} to the generator which produces electricity (see Fig. 4).

The mechanical power, extracted by the turbine, can be calculated by:

$$P_{mec} = \frac{1}{2} C_p(\lambda, \beta) \rho A V_{tidal}^3 \tag{1}$$

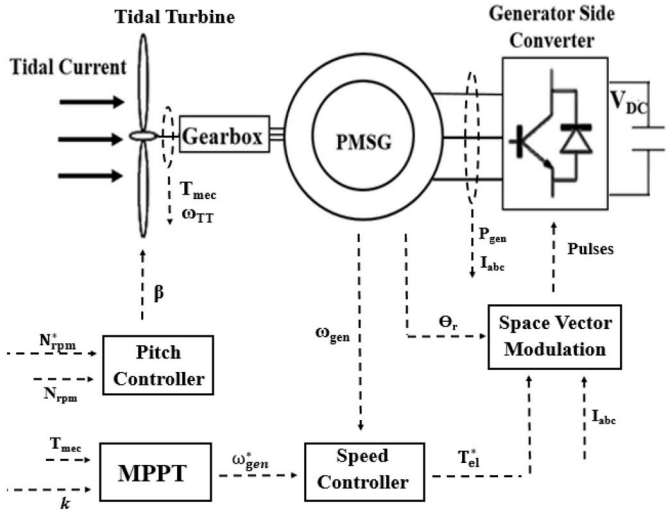

Fig. 4. Block diagram of the control system for single turbine.

Where ρ is the density of water in kg/m^3, and A is the rotor swept area in m^2. The sea water density is assumed constant at 1024 kg/m^3 and the swept area is based on a 11.5 m blade. V_{tidal} is the actual flow velocity in m/s. C_p is the power coefficient which is a function of TSR, λ and blade pitch angle β, in degrees. The TSR, defined as the ratio of the speed of the blade tips over the incoming tidal flow velocity:

$$\lambda = \frac{R_t \omega_{TT}}{V_{tidal}} \tag{2}$$

Where ω_{TT} is the angular speed in rad/s of turbine and R_t is the rotor radius.

The TCT modelled in this paper is a hypothetical turbine. Utilize the numerical tool of HARP_Opt which combines multiple-objective genetic algorithm and blade-element momentum theory flow model to design the turbine rotor [36]. This tool calculated the C_p curve of the turbine, turbine rotor inertia and gearbox ratio. The specifications of this turbine used are given in Table 1 and the $C_p(\lambda, \beta)$, curve in Fig. 5.

TCTs tend to have a cut-in speed, with a period of enforced idleness at low flow velocity periods; in this model, the cut-in flow velocity set to 1.0 m/s and the rated flow velocity is 2.5 m/s. When the flow velocity is below or at the rated value of the turbine, the rotation speed of the turbine rotor changes with the flow velocity. Thus, the value of TSR also changes in order to achieve maximum power extraction. Meanwhile pitch angle, β, is kept constant. For reference this is chosen to be the 0°. The optimal TSR derived from the power coefficient curve is 7.95, which

Table 1
Tidal turbine parameters.

Parameter	Symbol	Value	Units
Rotor radius	R_t	11.5	m
Maximum power coefficient	C_p	0.4778	–
Cut-in velocity	$V_{cut\text{-}in}$	1.0	m/s
Rated velocity	V_{rated}	2.5	m/s
Rated power	P_{rated}	1.5	MW
Optimal tip-speed ratio	λ	7.95	–
Gearbox ratio	r	66.667	–

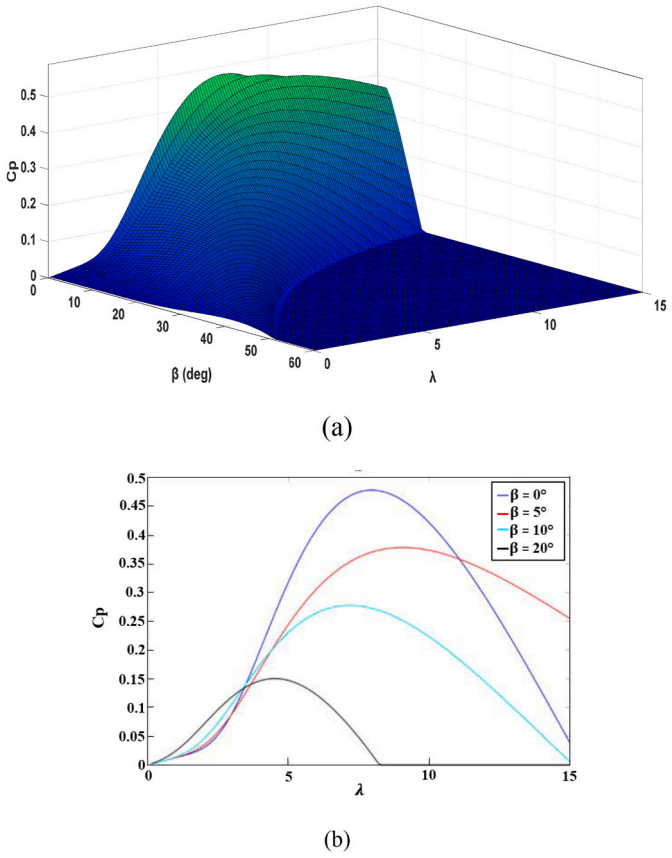

Fig. 5. Power coefficient C_p curve for the modelled turbine (a) 3D plot of $C_p(\lambda, \beta)$ as a function of TSR and blade pitch angle; (b) $C_p(\lambda)$ plot for different pitch angles.

gives an optimal power coefficient, C_p, of 0.4778. The blue line shown in Fig. 5 (b) presents the $C_p - \lambda$ curve when β is zero degree. Once the flow velocity increases above 2.5 m/s, the pitch angle is controlled to change with flow velocity; through increasing or decreasing the pitch angle, the value of C_p drops and deviates from the maximum point. As can be observed in Fig. 5 (a), pitching the blades by 20° drops C_p to nearly zero. The aim and design of the speed and pitch controller is presented in the following section.

2.2.2. Pitch controller

The purpose of a pitching mechanism is to ensure, at all times, that the output power does not exceed its rated value during periods of high flow velocity. The blades can be pitched to feather as the flow velocity increases. This reduces the lift force on the blade; therefore, the torque on the rotor is reduced and power is regulated.

A pitch controller was established in this model to control the amount of mechanical power captured. The control structure of pitching system as shown in Fig. 6.

This modelled pitch controller utilizes a closed loop control theory. Through comparing the rated generator speed, ω_{rated}, and the actual measured speed, ω, a pitch angle signal was produced. C_p reduces with the changing pitch angle, limiting the turbine speed to rated speed. As the direction of the upstream flow is not considered in this project, the pitch controller can only be used in regulating output power.

2.2.3. Maximum power point tracking

1). Maximum power point curve

Conventional MPPT control strategy is widely used in tidal turbines to extract maximum power from a tidal channel. In this proposed turbine model, a maximum power point curve which consists of optimized operating points at different values of flow velocity are firstly defined. The maximum power point curve modelled in this paper is based on equation (3) where the coefficient k is a constant equal to 1.1486 and is shown in Fig. 7.

$$T_{opt} = k \times \omega_{opt}^2 \tag{3}$$

Where T_{opt} is optimal mechanical torque in N·m and ω_{opt} is optimal generator speed in rad/s.

2). Speed controller

The speed and torque of the generator have to correspond to optimized operating points in this maximum power point curve. As mentioned above, when flow velocity experienced by the turbine is below or at the rated value, the turbines operate at maximum power coefficient (pitch angle and TSR are maintained at the optimum value, 0 and 7.95 respectively). By increasing generator torque to decrease rotor speed, the generator speed can be kept at a constant 1000 rpm. The pitch controller and speed controller work together to ensure that the

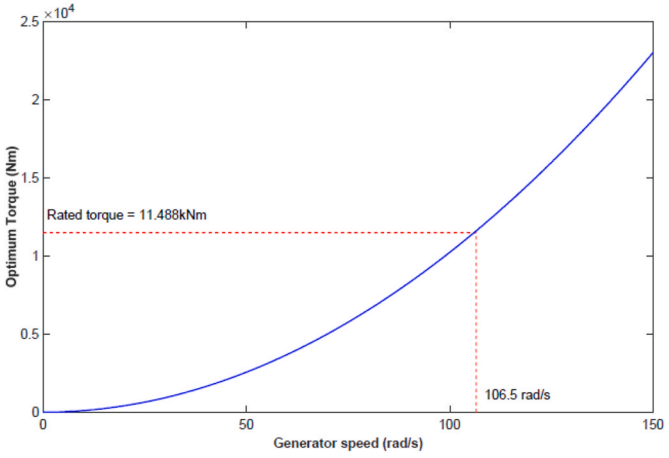

Fig. 7. Maximum power point curve for this TCT.

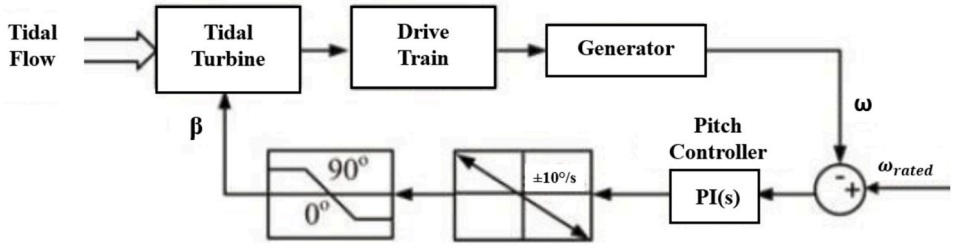

Fig. 6. Block diagram of the pitch controller.

output power does not go beyond the rated 1.5 MW in high flow velocity. A block diagram of the speed controller is shown in Fig. 8.

The optimal generator speed, ω_{opt}, generated based on equation (3), is used as a reference speed signal input to the speed controller. This reference signal is compared with the actual generator speed ω_{gen} to produce a reference electromagnetic torque, T_{el}*. Then T_{el}* is used as input to generator controller to trigger the gate signal of switch devices in the rectifier to control the rotational speed of generator.

2.2.4. Mechanical loads on turbine rotor

As the mechanical components, such as the turbine blade, shaft and support structure, are not modelled within Simulink, the estimation of hydrodynamic loads on TCTs is based on axial momentum theory. In this theory, the rotor which comprises a number of blades rotating about a centre hub is simply treated as a porous disc which presents a uniform resistance to the flow passing through it; actuator disc models have been widely used in theoretical and numerical studies of tidal current power [37].

Mathematical modelling is used for calculating the thrust, torque and power coefficients. It should be noted that only the contribution of variations in the vertical profile of the tidal flow to the operational fatigue loading on the tidal turbine blades is investigated in this paper.

As the use of axial momentum theory does not take into account of three-dimensional flow effects and the structure of the turbine blades, there may be a loss in accuracy for the estimation of loads [37]. However, it is able to present the variations of loads with incoming flow velocity which helps to achieve the one objective of this study – the mitigation of fatigue loads. The implementation of this numerical model is also more straightforward and can be easily integrated with the electrical model in Simulink.

A modified momentum theory proposed in Ref. [38] is used in order to achieve a more realistic loading prediction. This modified theory accounts for the rotation of the fluid within the slipstream, which gives insight into the relationship between the TSR and thrust and torque coefficients. The power coefficient, C_p, is a function of the axial induction factor and is given by:

$$C_p = 4a(1-a)^2 \tag{5}$$

The axial-induction factor, a, is the fractional decrease in flow velocity between the freestream and the turbine rotor. This coefficient, a, is related to C_p by the momentum theory [39]. This suggests that a maximum C_p value exists depending on the choice of a. The torque coefficient, C_Q for a tidal turbine is commonly defined as,

$$C_Q = \frac{Q}{0.5\rho\pi V_{tidal}^3 R_t^3} = \frac{4a(1-a)^2}{\lambda} \tag{6}$$

Where, Q is the torque on turbine.

The thrust, T is the axial force applied by the tidal current on the rotor of a tidal turbine. The thrust coefficient, C_T, is defined to be the ratio of the thrust on the turbine disc to the freestream dynamic pressure multiplied by the area of the turbine disc. Applying the definition of the axial induction factor, the thrust coefficient can be written as:

$$C_T = \frac{T}{0.5\rho V_{tidal}^2 A} = 4a(1-a)\left[\frac{2a(1-a)}{\lambda^2}+1\right] \tag{7}$$

From the above equations, altering the TSR and/or pitch angle will affect power, thrust and torque coefficients. It can be observed that a slight decrease or increase in a has a much greater impact on C_T than on C_p. Therefore, the operating point of the tidal turbine is approaching the maximum tidal current energy utilization efficiency when a is properly reduced or slight increased.

Although it has a slight adverse effect on the power coefficient, the thrust coefficient can be significantly reduced. This is vital for the optimization process of choosing TSR and pitch angle, which will be discussed in section 3.

2.3. Turbine array model

The array comprises two upstream turbines, A1 and A2 separated by 3D centre-to-centre. A downstream turbine, B1 is located centrally between these, 4.5D downstream. Three turbines are arranged in a staggered layout, as shown in Fig. 1.

These three turbines enable a typical wake situation within an array to be presented; transport time delay of downstream flow velocity to B1 depends on the distance between two rows and instantaneous flow velocity directly behind first-row turbines. Under multiple wake effects from two upstream turbines, the incoming flow velocity of B1 is much lower than the freestream velocity. In addition, for the purposes of this study, the use of three turbines can reduce computation time significantly. Wake prediction in this Simulink model will be presented in this subsection.

2.3.1. Wake prediction

Wake prediction for a real turbine is known to be complicated. In this proposed TCT array, an analytical method which was inspired from theoretical works of a ship propeller jet is used to simulate downstream flow velocity. This wake model refers to previous work presented in Refs. [40,41].

This wake model has been validated by comparing with another set of CFD simulation results from Creech et al. [42]; the 5% error between results was deemed to be within an acceptable margin [43]. The downstream energy loss calculated by this wake model depends on the value of a for upstream turbines and the recovery rate of tidal flow. In other words, downstream flow speed varies with the pitch angle and tip speed ratio of upstream turbines; this corresponds to a realistic turbine wake profile. Ambient turbulence intensity and transport delay are also taken into consideration.

In this model, the actual tidal current measurements at the EMEC is used as freestream flow (Fig. 7). A time delay calculation was employed using a study by Saunders in Ref. [44]; Simulink variable time delay blocks were used to model dynamic tidal current inflow for each waked turbine. These blocks delay the incident flow speed for each waked turbine according to the thrust coefficient, flow speed, and the distance between them. The inflow velocity for each turbine in this tidal array

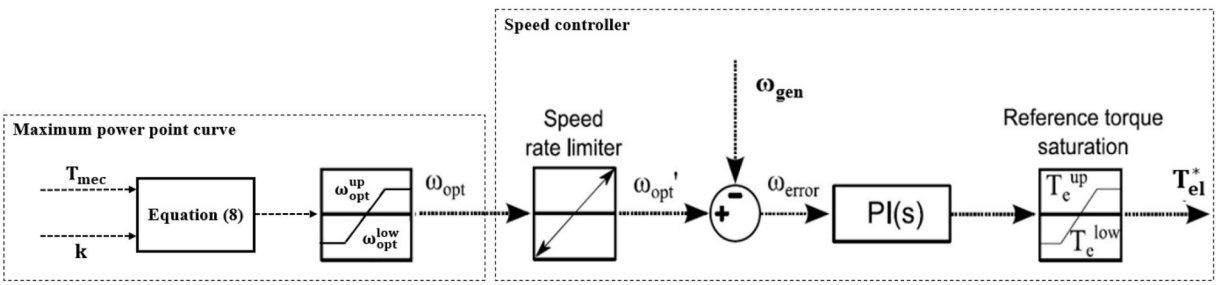

Fig. 8. Block diagram of the maximum power point curve and speed controller.

will be shown in section 6 with simulation results (Figs. 15 and 18).

2.3.2. Grid connection

The proposed TCT array model uses a DC collection system configuration, with turbines sharing a common DC link. The advantage of this configuration is to eliminate the individual turbine rectifiers, which can substantially improve the capital cost of the array [45,46]. All power generated by array is collected at a common DC link where the voltage is kept constant at 1800V. Then, DC power is converted back to AC again through an inverter. This array is finally connected to the grid after the voltage is stepped up from 690 V to 11 kV through a transformer. The structure of this grid connection scheme is shown in Fig. 9, where a single line represents the three-phase system.

3. Tidal current turbine array controller

3.1. The overall array control system

Axial induction factor control aims to reduce the wake deficit downstream by changing the axial induction factor of upstream turbines. This can be achieved by de-rating the upstream turbines, either by adjusting pitch angle and/or operating at a suboptimal TSR.

The flow velocity used in this paper is measured by ADCP in an actual tidal channel. Normally, Doppler devices are located at around 10–20 m ahead of the turbine so that flow velocity can be measured a few seconds before it reaches the turbines [47–49]. The exact time is dependent on the instantaneous flow velocity and the distance between the ADCP and the turbine. Even though measuring flow velocity is not the scope of this paper, it is an important measurement for the execution of the AIF control strategy.

The proposed array controller is able to optimize and determines new speed and pitch angle reference signals for each turbine before the measured flow velocity reaches the turbines; this allows turbines to quickly respond the upcoming flow velocity input. In low flow velocity ($V_{in} < 2.5$ m/s), the goal of fatigue loads mitigation is mainly achieved by varying the rotor speed. The variation of pitch angle is negligible due to the array controller also needing to ensure enough power extraction.

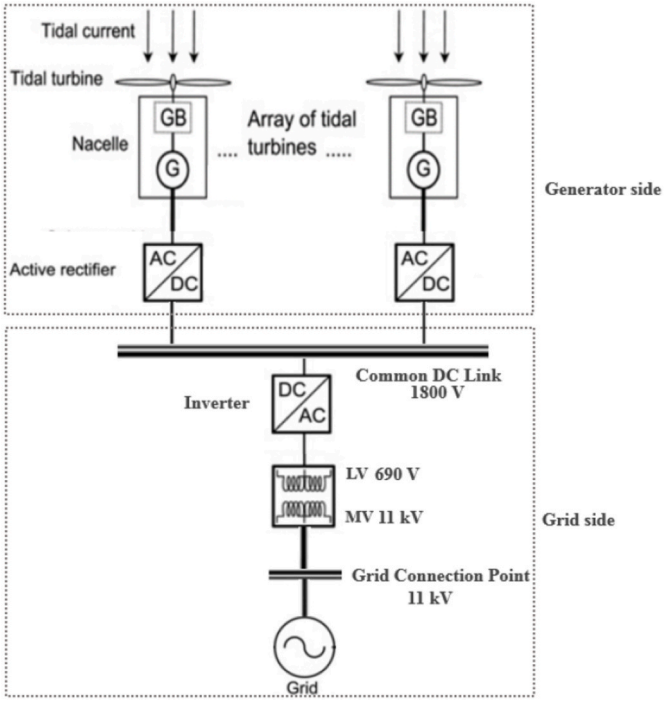

Fig. 9. Electrical configuration of a tidal array with shared common DC link.

In high flow velocity ($V_{in} \geq 2.5$ m/s), the array controller provides speed and pitch angle reference for each turbine control system.

The overall control system is shown in Fig. 10. The array controller takes measured flow velocity as an input to generate new TSR, λ^*_{new}, and pitch angle, β^*_{new}, reference values. These optimized reference values are applied to the Simulink model to produce outputs; total power, P_{total}, and mechanical loads, Q_n and T_n.

3.2. Array controller

3.2.1. Flow velocity process

One specific time period of flow velocity can be measured by the ADCP before it reaches the turbine. The proposed array controller will decide the new λ and β references for this time period of flow velocity and then decide new references for the next and following time period of flow velocity. In other words, the whole tidal cycle is treated as a number of small sections of flow velocity for optimization. The proposed array control strategy constitutes 4 parts; read and process flow velocity, optimization, evaluation and prediction, and results combination and selection.

The execution of the array control strategy starts with averaging the measured time-variable flow velocity in one time period. Based on this averaged flow velocity, the corresponding λ and β can be easily decided from the C_p (λ, β) curve as shown in Fig. 2. The determination of the averaged TSR and β is important for the following optimization, since these two values will be used to decide the upper and lower limits of the change of rotor speed and blade pitch angle.

3.2.2. GA optimization

In this paper, the optimal pitch angle and tip-speed ratio settings for each turbine are determined using a genetic algorithm (GA), which contains multiple objective and constraint functions. Firstly, objective functions are defined; for the purpose of this study, maximizing output power whilst reducing mechanical loads on turbine blades, multi-objective optimization is required. Equations (3), (6), (7) and (9) are used as objective functions to optimize each turbine's power, torque and thrust and optimize total array power respectively. In a conventional MPPT control strategy, mechanical loads change with flow velocity. However, in AIF control the optimized loads are expected to be kept at a relatively stable level, which implies that loads need to increase or decrease on the basis of the original MPPT results to mitigate their fluctuation. When the flow velocity exceeds the average value, the corresponding loads need to be reduced. Conversely, loads will be increased when the flow velocity drops below the average value. Secondly, the constraints for objective functions are established. The multi-objective GA searches for optimization results based on a set of constraints. Three variables, λ, β and induction factor, a, determine the optimization results. As mentioned in section 2, slight variations of λ and β can cause significant reductions in power and loads. Therefore, the boundary constraints of these variables need to be chosen carefully to ensure the code is able to generate proper solutions that guarantee enough power is extracted. The allowable maximum power reduction can be adjusted based on requirements, for example, the status of the grid. In this paper, the mitigation of fatigue loads is based on an allowable maximum 5% power reduction.

$$P_{total} = \sum_{i=1}^{n} P_{TT_i} \tag{9}$$

As a GA is a random-based evolutionary algorithm that search optimal results based on constraints, it is important to evaluate these optimization results and select the most appropriate λ and β for each turbine. In this proposed array controller, all possible results that meet the constraint of maximum 5% power reduction are considered. Fig. 11 shows the maximum and minimum allowable values of TSR when a 5% power reduction is allowed. It is worth noting that the percentage of

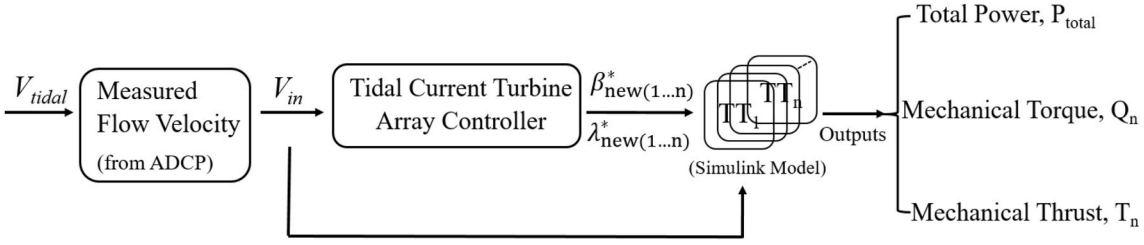

Fig. 10. Overall control system.

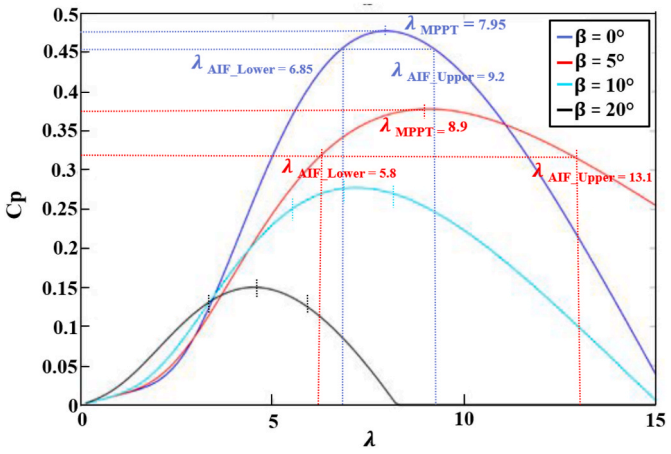

Fig. 11. Tidal turbine power coefficient curves versus tip-speed ratio for different blade pitch angles. The maximum and minimum limits of TSR shown for the AIF control strategy compared to the MPPT control strategy.

allowable power reduction can be adjusted based the different requirements. For example, the output of each turbine within an array can be controlled based on the amount of power that grid operators require.

The GA code is run several times, each time the bounds of the three variables are adjusted slightly and appropriate results are chosen. All results are used to the following prediction and combination part.

3.2.3. Evaluation and prediction

After the GA optimization, all optimal λ and β within the given constraints are selected for each turbine. These different optimal results will generate different array outputs. There is no doubt that all these results enable to mitigate fatigue loads for the turbine more or less, whilst ensure enough power is extracted. Some results are able to improve output power at the cost of slightly higher fatigue loads; for example, increase rotational speed but decrease pitch angle on the basis of MPPT control would increase loads on turbine rotor also increase power, due to power equals to torque times rotational speed. But under the control of some results, a reduction in blade fatigue damage at the expense of maximum power captured. This is caused by lower rotor speed bigger pitch angle in the AIF control.

According to structural load analysis, pitching the blades to reduce the power has little effect on reducing loads when the flow velocity is below the rated value. However, adjusting the speed considerably decreases the fluctuation of structural loads. At above rated flow velocity, an increase in pitch angle has greater effect than adjusting the λ on fatigue load mitigation. Therefore, choose the optimal results of small β and large λ when $V_{in} < 2.5$ m/s, where the β should as close to zero as possible; conversely, optimal results with large pitch angle would be the preferred option when $V_{in} \geq 2.5$ m/s.

In a TCT array, any changes of λ and β on upstream turbines will affect the input of downstream turbines. Therefore, the one set of optimized results for one upstream turbine corresponds to one particular downstream flow velocity and array outputs. In this paper two turbines, A1 and A2, are located at the first row A; it is assumed that both of them operate at the same optimized λ and with a chosen small optimized value for β, which means they will produce more power but with relatively high fatigue loads. Meanwhile, less power can be extracted by the downstream turbine, B1. Conversely, a large β means more power left for B1 but with an increase downstream flow turbulence and larger load fluctuations on B1 correspondingly. Even though turbines at the same row have the same or very similar incoming flow velocity input, it is not necessary for them to have identical optimized λ and β references; by assigning different optimized results for turbines on the same row, there is a potential to improve the performance of the whole array further. Here, the optimal results of each turbine are combined to predict all possible array outputs and select the most appropriate results for the array in this time period of flow velocity. Also, optimizing the outputs of each turbine in an array does not ensure that the whole array output will definitely be improved. For example, operating some of the turbines with MPPT control may lead to better array output. The selected results, β^*_{new} and λ^*_{new} are assigned to each the control system for each turbine, which are able to maximize the whole array output averaged over one time period and also mitigate fatigue loads. Fig. 12 shows the diagram of the array controller.

The power extracted by a turbine depends on the mechanical torque, T_{mec} and turbine rotor speed, ω_{TT}. The optimized λ and β will generate new mechanical torque, $T^*_{mec\_new}$ and new rotor speed, ω_{TT_new}. In order to ensure turbines are able to track the new λ and β references, the modifications of original pitch and speed controller are required.

Every turbine model in this array is connected to the PMSG through a gearbox, changes in the speed of the low-speed shaft of the turbine affects the high-speed shaft of generator, ω_{gen}. Therefore, the change in turbine rotor speed requires the generator to response accordingly. The modification of the speed controller is based on varying the coefficient k, forcing the generator to follow a different reference speed. The new coefficient k, k_{new} is calculated by equation (8), both $T^*_{mec\_new}$ and ω_{TT_new} are decide the k_{new}. Since the turbines no longer operate at optimum TSR in AIF control, by decreasing coefficient k the generator speed start to increase to comply with a higher ω_{TT}. Conversely, increasing k the generator speed, ω_{gen} will decreases due to lower ω_{TT}.

In a pitch controller, the pitch angle is decided by the error between the reference generator speed and actual speed. In the AIF control, a new generator speed reference $N^*_{rpm\_new}$, that decided by the new λ. It is used as the reference signal to compare with the actual generator speed, in order to track the new β. Fig. 13 shows the block diagram of the AIF control method that explain how to modify the conventional MPPT control to implement this method in a simulation model.

After completing the optimization for this period of flow velocity, the array controller repeat above optimization process for the next and following incoming flow velocity. Detailed presentation and discussion of results will be shown in the next section.

4. Results and discussion

The simulation model of a TCT array and corresponding array controller are established; the control system for each turbine has been

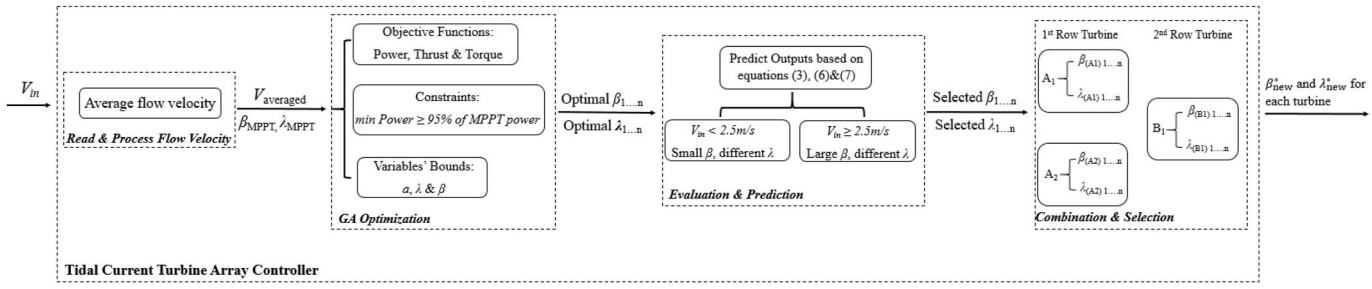

Fig. 12. Schematic diagram of the array controller.

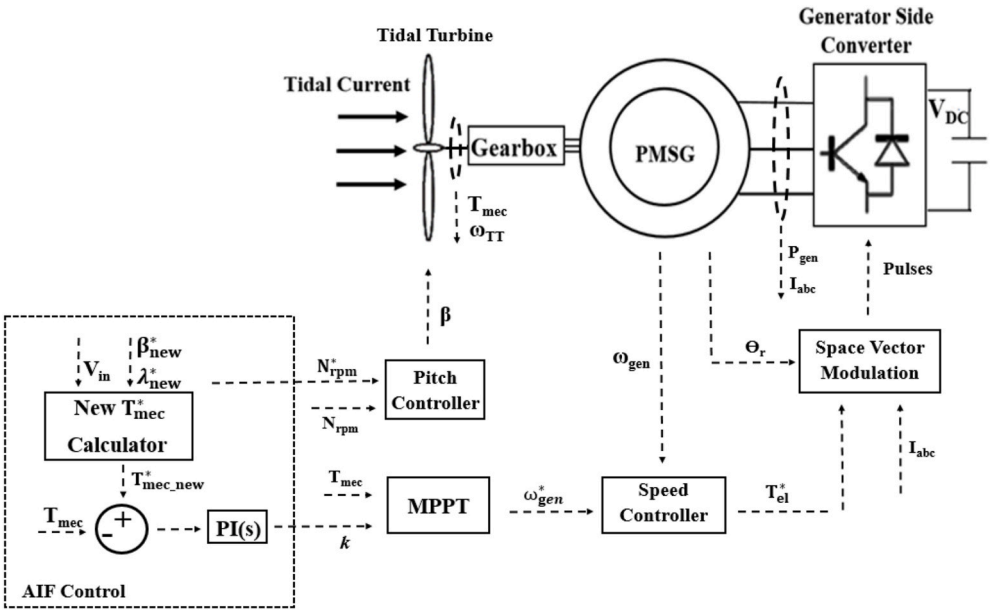

Fig. 13. Block diagram of the control system for single turbine under AIF control.

modified to follow optimized speed and pitch angle signals. In this section, more details regarding the performance of the array under the axial induction factor control strategy is presented. It assesses the dynamic response of the controller in temporally-variable flow speed by comparing to the MPPT control strategy in terms of output power and the variation of torque and thrust. At the same time, this section investigates the possible effects of this novel control strategy on the electrical subsystems.

4.1. Optimization and simulation results

4.1.1. Upstream turbines

In this paper, a real tidal flow velocity is used as the input. Fig. 14 shows corresponding optimization and simulation results of the two upstream turbines, A1 and A2. The incoming flow velocity is presented in Fig. 14 (a); identical flow velocity is assumed for A1 and A2, which varies between 2.1 m/s and 2.9 m/s within a time period of 120 s.

Blade pitch angle under MPPT and AIF control are shown in Fig. 14 (b). When $V_{in} < 2.5$ m/s, β is always kept at zero degrees for the MPPT control strategy. However, under the AIF control strategy, β is increased from zero degrees in order to decrease loads on the turbine rotor. Limited by the requirement of 5% allowable power reduction, β^*_{new} only varies between 0 and 0.9°. When $V_{in} \geq 2.5$ m/s, the blades start to pitch and β increases with the flow velocity. Compared with the MPPT control strategy, β in AIF control increased by approximately an additional 2–5°. Optimization results have shown that higher flow velocity generally corresponds to a larger β^*_{new}. Observing Fig. 14 (b), it can be seen that β^*_{new} for A1 is higher than that in A2 by around 0.5–1°. This is because the proposed array controller optimizes all turbines as a whole rather than individual turbines. A larger pitch angle means that this turbine is not able to extract maximum power as usual since more extractable energy is left for downstream turbines. Reduction in output power of upstream turbines and the increment in output power of downstream turbines have potential to increase the whole array output, which will be shown in detail and discussed later.

Fig. 14 (c) shows the variation and comparison of the new generator speed reference for A1 and A2 in MPPT and AIF control. The determination of the value of optimal λ not only depends on incoming flow velocity, but also the average flow velocity over a certain time period; when the instantaneous flow velocity exceeds the average flow velocity, the generator needs to accelerate to reduce mechanical loads. For example, the optimal generator speed reference of turbine A1 (red dashed line) during 40–60 s is increased to 1100 rpm, which is higher than the MPPT rated speed of 1000 rpm. The opposite situation can be observed when instantaneous flow velocity falls below the average value, where the generator rotates slower than in MPPT control. Lower rotational speed results in higher mechanical load. The increase and decrease of torque and thrust allows the mitigation of load fluctuations, and subsequently the mitigation of fatigue loads. Turbine A1 and A2 have similar optimal speed but greater change of speed of A2 can be observed, which means the generator of A2 requires a faster response.

According to equations (6) and (7), mechanical torque and thrust change with tidal flow; torque and thrust increase with the cube and square of the flow velocity respectively. Therefore, torque and thrust

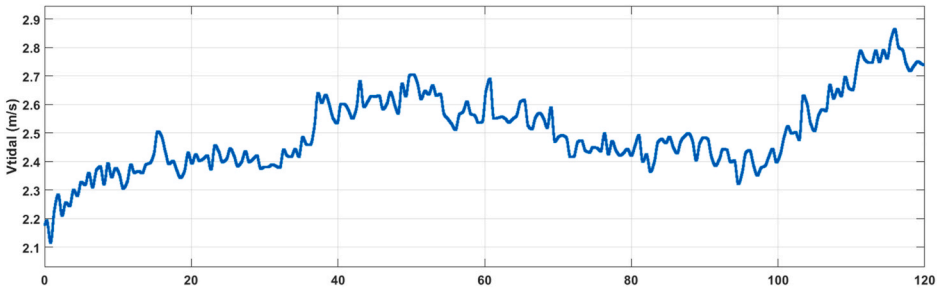

(a)

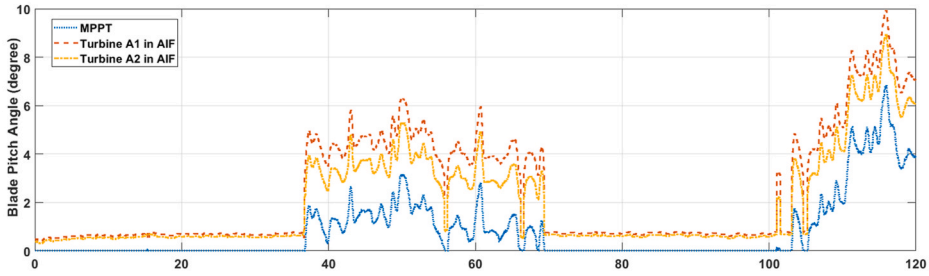

(b)

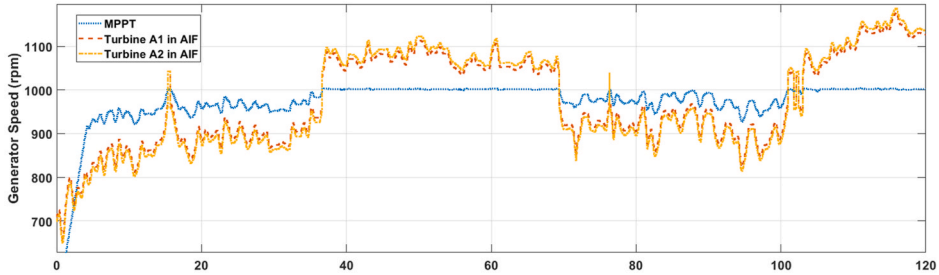

(c)

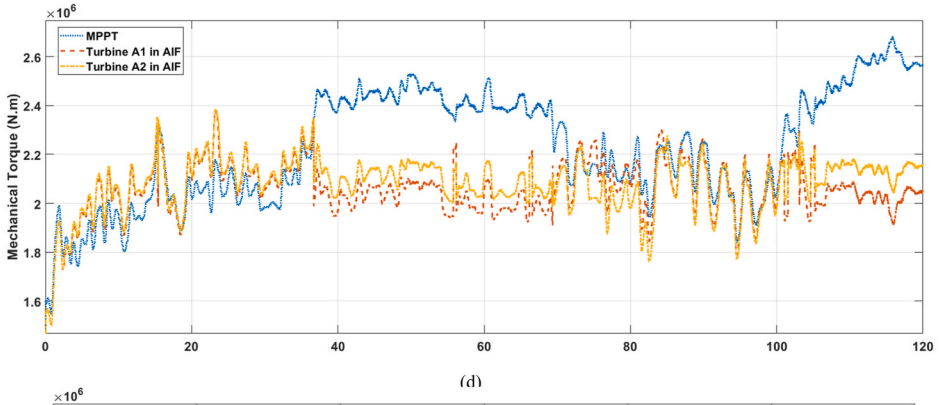

(d)

(e)

Fig. 14. Comparison of MPPT and AIF results for upstream turbines A1 and A2. (a) Incoming flow velocity, (b) Blade pitch angle, (c) Generator speed, (d) Mechanical torque, (e) Mechanical thrust.

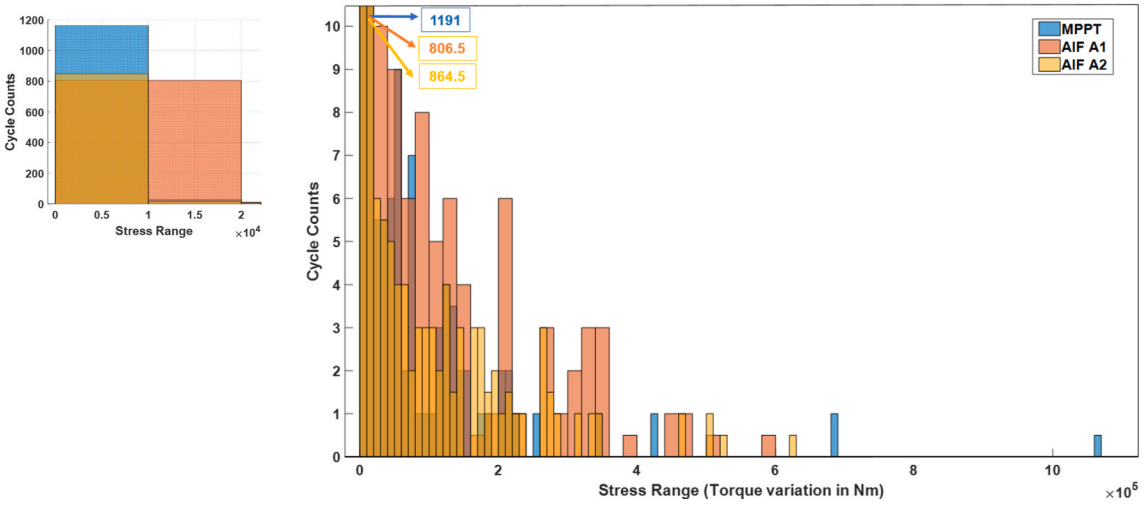

Fig. 15. Rainflow counting for fatigue torque analysis for upstream turbine A1 and A2. The stress range bins include all torque variations from the previous bin value up to the range indicated.

have the same variation trend but the value of torque is greater than thrust, which can be observed in Fig. 14 (d) and (e). Between 20 and 40 s, due to lower optimal reference speed and greater pitch angle, the generator is controlled to rotate slower in AIF control, resulting in an increase in torque for A1 and A2, exceeding the torque value for MPPT control. Conversely, during 40–60 s, the generator rotates faster, resulting in lower torque. The torque is controlled to increase or decrease on the basis of the original MPPT in order to mitigate its fluctuation. Therefore, in AIF control the optimized torque is kept at a relatively stable level. Similarly, the AIF control strategy also affects the variations of thrust. However, compared with the changes in torque, the variation of thrust reduces less; during the time period of 0–30 and 70–100 s where $V_{in} < 2.5$ m/s, the curve of the optimal and MPPT thrust are almost overlapped. A slight reduction can be observed in the time period of 40–60 and 110–120 s where $V_{in} \geq 2.5$ m/s.

In general, the effect of AIF control strategy on the changes on thrust is less than that on torque due to a difference in sensitivity of torque and thrust on tidal flow and axial induction factor. In order to assess the AIF control strategy, the rainflow counting method for fatigue analysis from MATLAB is used. Rainflow counting for mechanical torque and thrust of turbine A1 and A2 for the whole simulation time period is presented in Figs. 15 and 16 respectively. It is to be emphasized that for large stresses which cause the deformation of turbine blades, failure occurs after much fewer stress cycles (low cycle fatigue).

Fig. 15 shows the reduction in stress range of torque from the 6.9e5 to 10.7e5 bins during MPPT to the 5.2e5 and 6e5 bins for A1 and to the 5.3e5 and 6.3e5 bins for A2. Fig. 16 shows the reduction in stress range of thrust from the 6.6e5 and 6.7e5 bins during MPPT to the 5.8e5 and 5.9e5 bins for A1 and to the 5.2e5 and 5.3e5 bins for A2. Moreover, high cycle fatigue when torque and thrust are in the range of 0 to 0.1e5 is also mitigated.

From these two figures, it can be observed that the AIF control does reduce the stress range for both torque and thrust; A1 has greater reduction compared to A2.

4.1.2. *Downstream turbine*

Due to the wake effect, incoming flow velocity for the tidal turbine B1, which operates downstream, decreased by 40%, compared with the freestream flow velocity. Also, the increase in turbulence intensity in the wake results in large unsteady loads on B1 and more fluctuations in the corresponding β^*_{new} and $N^*_{rpm\_new}$ signals. Fig. 17 presents the optimization and simulation results of B1 in MPPT and AIF control.

The incoming flow velocity presented in Fig. 17 (a), which is always below the rated value of 2.5 m/s, varies between around 1.4 m/s and 2 m/s. Similarly for changes in A1 and A2, β is always kept at zero degrees for the MPPT control strategy. However, under the AIF control strategy,

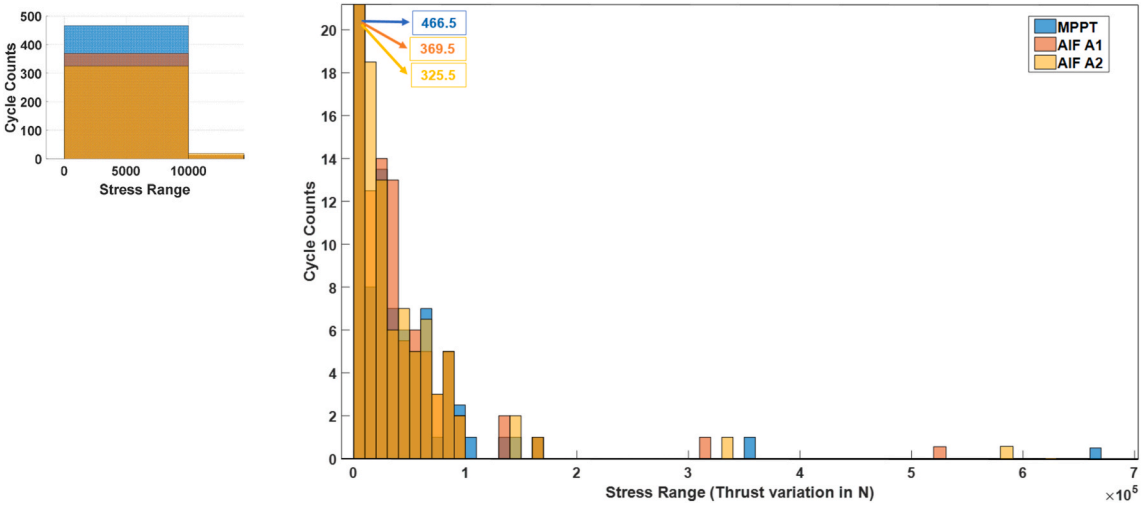

Fig. 16. Rainflow counting for fatigue thrust analysis for upstream turbine A1 and A2.

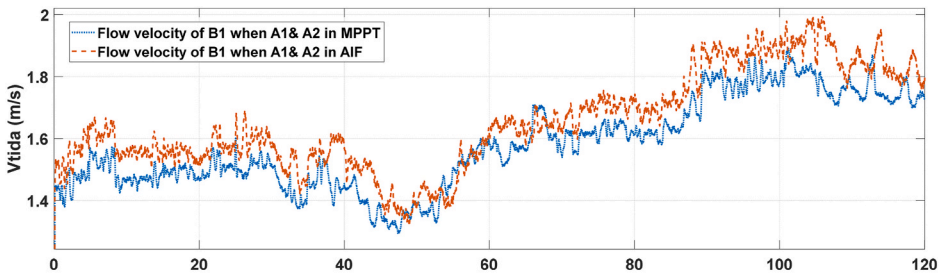

(a)

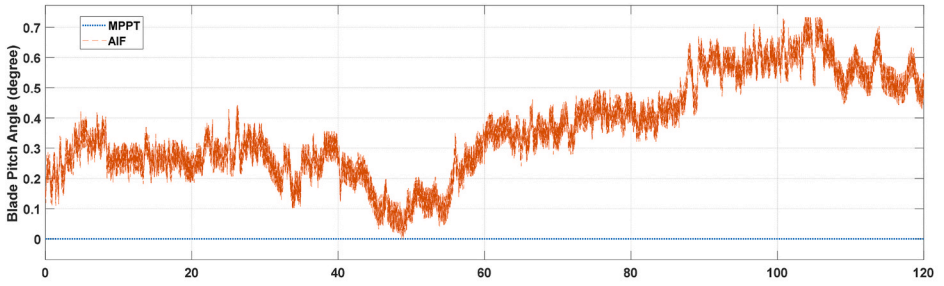

(b)

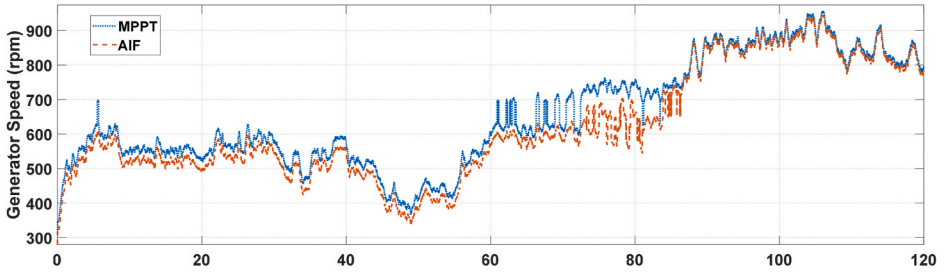

(c)

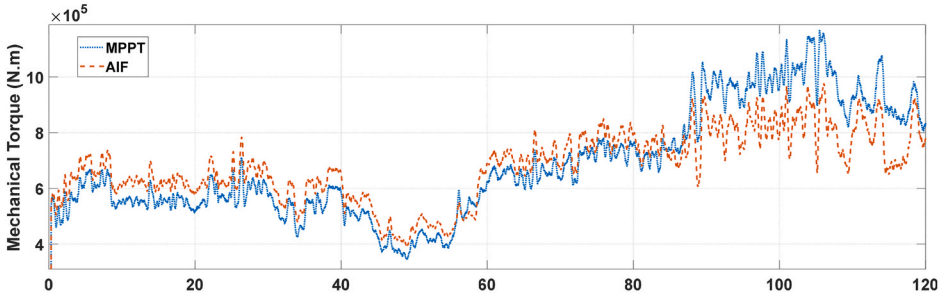

(d)

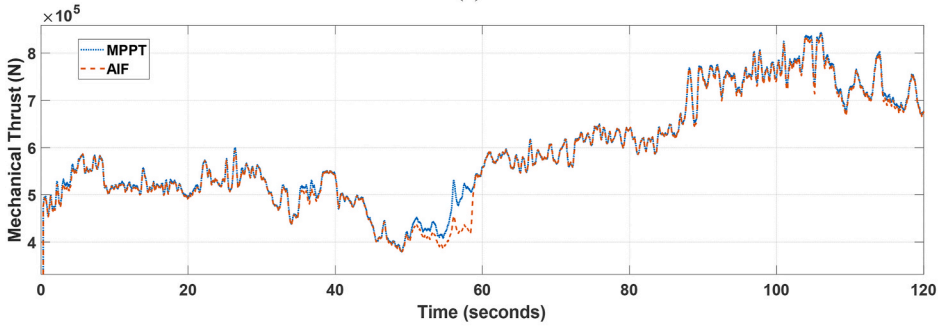

(e)

Fig. 17. Optimization and simulation results of downstream turbine B1 in MPPT control and AIF control. (a) Incoming flow velocity, (b) Blade pitch angle, (c) Generator speed, (d) Torque, (e) Thrust.

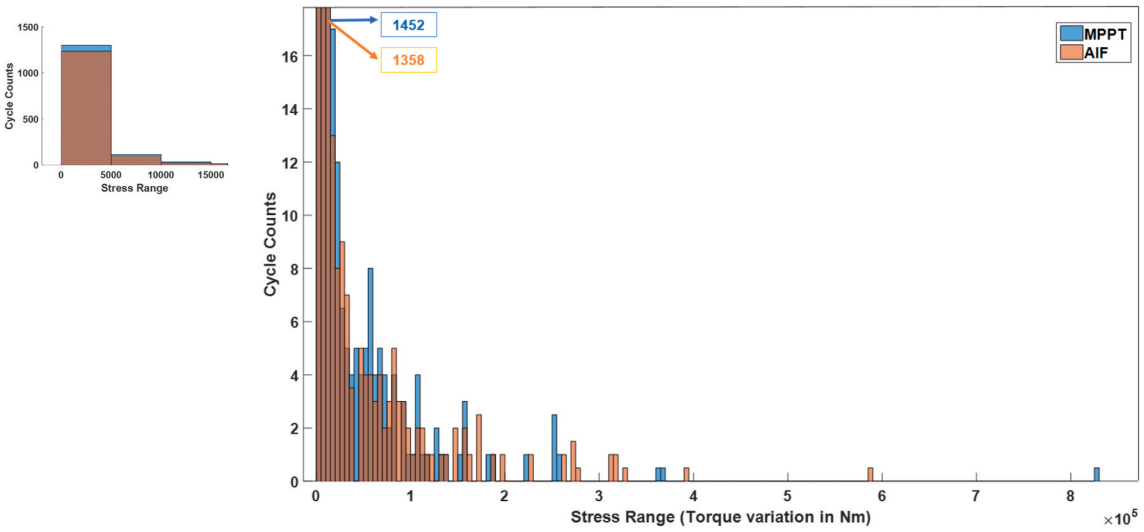

Fig. 18. Rainflow counting for fatigue torque analysis for upstream turbine B1. The stress range bins include all torque variations from the previous bin value up to the range indicated.

β is increased and varies between 0 and 0.9°, which can be observed in Fig. 17 (b). Fig. 17 (c) shows the variation and comparison of new generator speed reference for B1. During 0–70 s, $N^{*}_{rpm\_new}$ of B1 is decreased below the MPPT speed. Conversely, the generator rotates faster during 70–120 s; higher rotational speed results in lower mechanical load.

Fig. 18 shows the reduction in stress range of torque from the 8.2e5 and 8.25e5 bins during MPPT to the 5.7e5 and 5.8e5 bins for B1. Fig. 19 shows the reduction in stress range of thrust from the 4.6e5 and 4.7e5 bins during MPPT to the 4.2e5 and 4.3e5 bins.

For both low and high flow velocity situations, the proposed AIF control strategy is able to mitigate fatigue torque on all turbines significantly. However, it has greater effect for high flow velocity.

4.1.3. Output power

Fig. 20 demonstrates the output power for each turbine and total array power in MPPT and AIF control. In this case the upstream turbines operated with increased blade pitch angle. While the energy production of the down-regulated turbine decreases, the flow velocity in their wake increases. This allows for a higher energy production at downstream turbines that could guarantee a higher level of power production. Red and yellow lines represent the output power of A1 and A2 in AIF control respectively, which are normally lower than the power produced in MPPT (blue line). Conversely, B1 is able to extract more power in AIF control. The purple and green lines represent the output power of B1 in AIF and MPPT control respectively. The total array output power is measured at the grid side. Energy extracted from tidal flow is delivered to the grid through an inverter and transformer, which introduce harmonics and cause power losses. Thus, the total array output power is lower than the sum of each turbine output power, and more fluctuations can be observed. Light blue and dark red lines represent the array output power in MPPT and AIF control respectively. Comparisons between MPPT and AIF control for array power are difficult to observe due to the large fluctuations of the instantaneous output power of the array. Therefore, average power over one time period needs to be known to verify that the AIF control strategy achieves a high level of power extraction after AIF control is applied.

Table 2 shows the average power of each turbine and the overall array over the 120-s time period. The average power of upstream turbines A1 and A2 in MPPT control is the same since they have the same incoming flow velocity; however, in AIF control turbine A2 produces more power than A1. This is caused by the different optimal β and λ

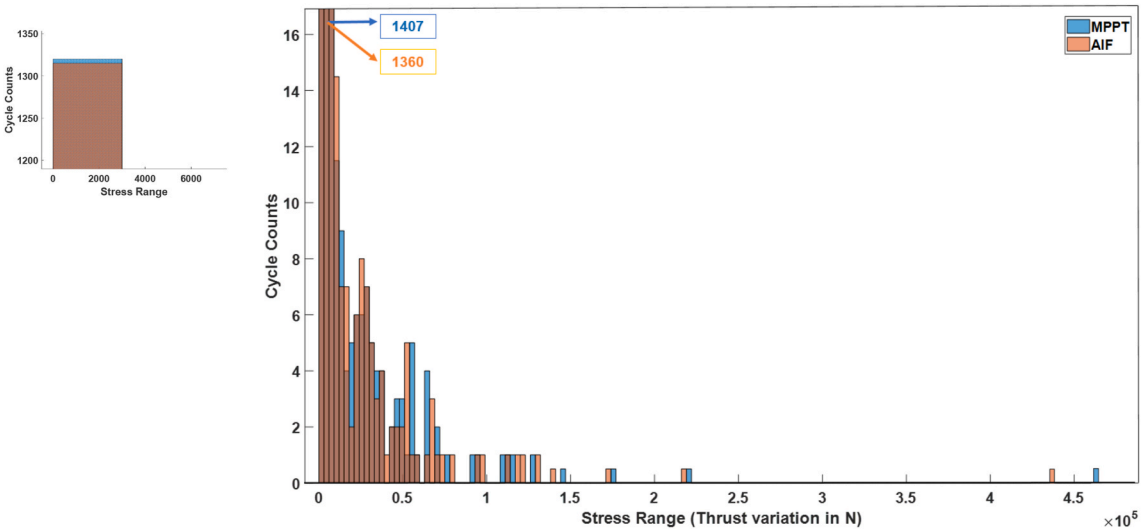

Fig. 19. Rainflow counting for fatigue thrust analysis for upstream turbine B1.

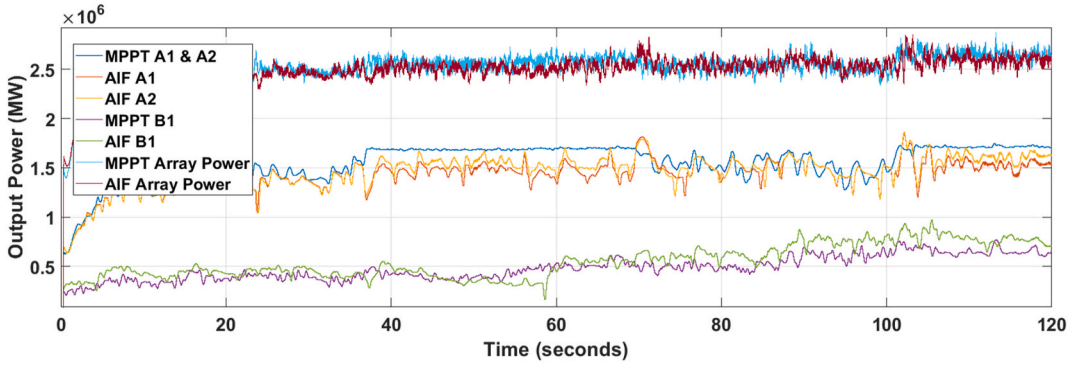

Fig. 20. Output power of each turbine and total array power in MPPT and AIF control.

Table 2
Average power over this 120-s time period.

Control Method	Turbine A1	Turbine A2	Turbine B1	Total Array Output Power
MPPT control	1.5426e6	1.5426e6	0.48102e6	2.5279e6
AIF control	1.4279e6	1.4568e6	0.55030e6	2.5060e6

settings; β^*_{new} of A1 is slightly larger than that of A2 which means less power is extracted by A1 and more extractable energy left for B1. Therefore, the average power of B1 in AIF control is increased. However, the increment of power in B1 is not enough to compensate the power reduction of the two upstream turbines A1 and A2. Therefore, the total array average power produced in AIF control is 0.87% lower than that in MPPT control. In the other words, the output total array power average over 120 s is similar for both types of control, with less than 1% difference.

4.2. Discussion

In comparison to other control strategies which change β or λ only, the proposed AIF control strategy controls both β and λ simultaneously to mitigate fatigue loads whilst guaranteeing a high-level output power extraction.

The simulation results indicate that the fluctuation of mechanical torque and thrust on all three turbines are reduced after the AIF control strategy is applied; this is particularly evident for mechanical torque where a greater reduction can be observed. It is noteworthy that turbines are more sensitive to AIF control in a high flow velocity situation. If generator speed increases by 40 rpm in both low and high flow velocity on the basis of corresponding MPPT speed, a large reduction on the variations of torque and thrust can be observed when $V_{in} \geq$2.5 m/s. This also explains why fatigue load mitigation on turbine B1 is less significant than that of A1 and A2 which have higher incoming flow velocity. The stress range of torque for all turbines is reduced by around 30–40% and the stress range of thrust is reduced 9–20%.

For a single turbine, we can observe that the torque and pitch controllers compete with each other; a reduction in blade fatigue damage is achieved at the expense of a reduction in power capture. However, if AIF control is applied in a turbine array, turbines are able to cooperate with each other to trade-off between power and fatigue damage. From simulation results, the output power of turbine A1 and A2 reduced by around 7% and 5.5% respectively. However, changes of β and λ on these two turbines result in more extractable energy being left for B1. Therefore, the power reduction of upstream turbines can be compensated by a power increase in downstream turbines; under the premise of reducing load fluctuations, less than 1% power reduction can be observed for this three-turbine array. If more turbines are placed downstream, the whole array output power may potentially increase on the basis of MPPT control.

In this paper, the benefits of this novel control strategy shown by the simulation results for an example three-turbine array is limited. In reality, hundreds of tidal turbines are typically deployed in an array. Therefore, a larger-scale array will be simulated to test the effects of this AIF control as a next step in this research.

It should be noted that the control strategy of adjusting either β or λ only was also tested in this turbine array model; to achieve this, the same $N^*_{rpm\_new}$ was assigned to the speed controller of turbines and the pitch controller was kept following the original reference signal produced in MPPT control. To adjust β only, the pitch controller follows β^*_{new} while the speed reference signal is generated by MPPT control. By controlling β or λ (but not both), both mechanical loads and output power have corresponding changes. However, these changes do not mitigate fatigue loads effectively and does not guarantee simultaneous high level of power extraction. For example, the thrust fluctuations even increase when only the generator speed is controlled and the output power is less than that in MPPT and AIF control. Furthermore, larger torque fluctuations can be observed when the control strategy attempts to adjust pitch angle only.

The performance of this proposed array controller is outlined with particular emphasis on the dynamic response in time-variable flow velocity and the trade-off between output power and fatigue loads. In low flow velocity, the objective of stabilizing the fluctuation of loads is mainly achieved by adjusting generator speed. Conversely, the pitch controller dominates the results of the array in high flow velocity.

Unlike other control strategies which adjust rotor speed to change λ, this proposed array controller mitigates fatigue loads from an electrical perspective through changing generator rotational speed; the operation of the turbine rotor and the generator are controlled to deviate from the optimal points. Generators need to follow the new reference signals with greater variation, which means they are required to accelerate and decelerate faster. This causes the speed controller to operate at its limits regarding the maximum change in speed per second, due to the physical limitations of the generator. Therefore, in order to ensure generators are able to respond correctly and promptly; the setting of maximum acceleration and deceleration rate in rpm/s in the controller needs to change to match to physical generator.

Moreover, AIF is achieved by allowing the generator rotational speed to reach up to 120% of the rated speed. Hence, care must be taken to ensure that the generator is able to operate at overspeed and does not exceed its design limits, which may otherwise affect the performance and lifetime of the generator. Typically, generators in tidal turbines are operated in variable speed and most of them allow overspeed operation, for safety reasons. An example of one type of PMSG designed by ABB used in wind turbines allows operation within the speed range of up to 150% of rated speed, and a maximum overspeed of up to 240%.

Therefore, the prerequisite of overspeed operation under AIF control is confirmation that the motor can run at the overspeed frequency

without being damaged or shortened life expectancy. Some generator features also need to be considered when running at overspeed, like bearing speed rating. Bearings should be able to safely operate when generator operate at an overspeed condition without heat build-up that could reduce operational life.

Even if the generator is able to withstand higher rotational speeds, a greater variation in speed can result in more fluctuating electrical power which could potentially impact stability and power quality in electrical power system. For example, voltage instability, frequency deviation and harmonic distortion are all issue to be aware of during development. Therefore, the assessment and discussion of electrical power quality under AIF control will be a key objective of future work.

5. Conclusion

An array controller has been presented in this paper, which enables the mitigation of fatigue loads whilst guaranteeing a high level of power extraction. This paper presents a novel strategy in tidal turbine array control that focuses on optimization of both power and loads simultaneously. According to the temporally-variable incoming flow velocity, the proposed control strategy optimizes and assigns the reference signals of β and λ for each turbine controller.

This array controller is applicable to any TCT array, provided that the size and arrangement of the array and the specification and characteristics of the turbine are known. Throughout this paper, a number of objectives have been achieved:

- The fluctuation of mechanical torque and thrust on all three turbines A1, A2 and B1 are reduced after the AIF control strategy is applied; the stress range of torque for all three turbines is reduced by around 30–40% and the stress range of thrust is reduced by 9–20%. Moreover, the fatigue load mitigation on the two upstream turbines A1 and A2 is more significant than that of downstream turbine B1.
- Under the premise of reducing load fluctuations, output power for the three-turbine array reduced by less than 1%. Although the output power of turbine A1 and A2 reduced by around 7% and 5.5% respectively after AIF is applied, this power reduction is compensated by a power increase in downstream turbines.

The limitations of this proposed array controller and recommendations for future work is described below:

- The need for fast controller response times to control β and λ

  The time taken for each turbine controller to respond to new reference signals from the array controller needs to be shortened as much as possible in order to ensure that each turbine operates with the correct β and λ values when the corresponding incoming flow velocity reaches the turbines. In other words, control systems need to reach steady state as soon as possible for one specific time period of flow velocity and then respond to the next and following time period of flow velocity.
- Assessment of the lifetime of the pitching system

  The pitch system is one of the components in a tidal turbine that has both high failure rates and long downtime. Under AIF control, blades need to be pitched more frequently in low flow velocity situations; β varies between 0 and 1°. Compared with MPPT control, it is always kept at zero degrees under the same situation. Hence, more frequent use of the pitching system may affect its lifetime. This important issue will be considered in future work.
- Higher accuracy for calculation of loads

  The classical momentum theory provides perhaps the simplest description of an axial flow turbine as it does not take the structure of the turbine rotor and three-dimensional flow effects. Therefore, more advanced turbine rotor modelling methods, like blade element momentum theory (BEMT) and computational fluid dynamics (CFD) which are able to offer more accurate description of turbine performance will be considered in future work.

CRediT authorship contribution statement

Yidan Zhang: Modelling, Simulation, Data processing and, Writing – original draft. **Jonathan K.H. Shek:** Supervision, Writing – review & editing, and Proofreading. **Markus A. Mueller:** Supervision.

Declaration of competing interest

The authors declare that they have no known competing financial interests or personal relationships that could have appeared to influence the work reported in this paper.

References

[1] P. Ouro, P. Dené, P. Garcia-Novo, T. Stallard, Y. Kyozuda, P. Stansby, Power density capacity of tidal stream turbine arrays with horizontal and vertical axis turbines, J. Ocean Eng. Marine Energy 9 (2) (2023/05/01 2023) 203–218.
[2] Deutsche WindGuard GmbH, Capacity densities of EUROPEAN offshore wind farms, Available: https://vasab.org/wpcontent/uploads/2018/06/BalticLINes_CapacityDensityStudy_June2018-1.pdf, 2018.
[3] P. Enevoldsen, M.Z. Jacobson, Data Investigation of Installed and Output Power Densities of Onshore and Offshore Wind Turbines Worldwide, vol. 60, Energy for Sustainable Development, 2021/02/01/2021, pp. 40–51.
[4] SeaGen-S 2MW Proven and commercially viable tidal energy generation, Available: https://atlantisresourcesltd.com/wp/wp-content/uploads/2016/08/SeaGen-Brochure.pdf, 2014.
[5] SeaGen turbine, Northern Ireland, UK, Available: https://www.power-technology.com/projects/strangford-lough/, 2020.
[6] Andritz Hydro, Tidal current turbines, Available: https://www.andritz.com/products-en/hydro/products/tidal-current-turbines.
[7] SIMEC ALTANTIS ENERGY, Simec atlantis energy unveils WORLD'S largest single rotor tidal turbine, THE AR2000. Available: https://saerenewables.com/simec-atlantis-energy-unveils-worlds-largest-single-rotor-tidal-turbine-the-ar2000/, 2018.
[8] Marine Scotland Assessment. (02/05), Case study: Nova innovation - Shetland tidal array, Available: https://marine.gov.scot/sma/assessment/case-study-nova-innovation-shetland-tidal-array.
[9] 2021, 05/08), World's most powerful tidal turbine, the O2, starts exporting clean power, Available: https://orbitalmarine.com/o2-power-generation/.
[10] A. Uihlein, D. Magagna, Wave and tidal current energy – a review of the current state of research beyond technology, Renew. Sustain. Energy Rev. 58 (2016/05/01/2016) 1070–1081.
[11] D. Lande-Sudall, T. Stallard, P. Stansby, Co-located deployment of offshore wind turbines with tidal stream turbine arrays for improved cost of electricity generation, Renew. Sustain. Energy Rev. 104 (2019/04/01/2019) 492–503.
[12] Cost reduction pathway of tidal stream energy in the UK and France, Available: https://ore.catapult.org.uk/wp-content/uploads/2022/10/Tidal-stream-cost-reduction-report-T3.4.1-v1.0-for-ICOE.pdf, 2022.
[13] TETHYS, Nova innovation - Shetland tidal array, Available: https://tethys.pnnl.gov/project-sites/nova-innovation-shetland-tidal-array, 2021.
[14] OFFSHORE ENERGY, MeyGen sets record with world's first 50GWh of electricity generated by tidal energy, Available: https://www.offshore-energy.biz/meygen-sets-record-with-worlds-first-50gwh-of-electricity-generated-by-tidal-energy/, 2023.
[15] SIMEC ATLANTIS ENERGY, Partnership agreed with general electric to develop the world's largest tidal stream turbine, Available: https://saerenewables.com/partnership-agreed-with-general-electric-to-develop-the-worlds-largest-tidal-stream-turbine/, 2019.
[16] J. Thiébot, N. Guillou, S. Guillou, A. Good, M. Lewis, Wake field study of tidal turbines under realistic flow conditions, Renew. Energy 151 (2020/05/01/2020) 1196–1208.
[17] N. Djama Dirieh, J. Thiébot, S. Guillou, and N. Guillou, "Blockage corrections for tidal turbines - application to an array of turbines in the Alderney race," Energies, vol. 15, no. 10. doi: 10.3390/en15103475.
[18] K.B. Shariff, S.S. Guillou, An empirical model accounting for added turbulence in the wake of a full-scale turbine in realistic tidal stream conditions, Appl. Ocean Res. 128 (2022/11/01/2022), 103329.
[19] C. Frost, C.E. Morris, A. Mason-Jones, D.M. O'Doherty, T. O'Doherty, The effect of tidal flow directionality on tidal turbine performance characteristics, Renew. Energy 78 (2015/06/01/2015) 609–620.
[20] R. Vennell, Realizing the potential of tidal currents and the efficiency of turbine farms in a channel, Renew. Energy 47 (2012/11/01/2012) 95–102.
[21] R. Vennell, The energetics of large tidal turbine arrays, Renew. Energy 48 (2012/12/01/2012) 210–219.
[22] I. Fairley, I. Masters, H. Karunarathna, The cumulative impact of tidal stream turbine arrays on sediment transport in the Pentland Firth, Renew. Energy 80 (2015) 755–769, 2015/08/01/.

[23] R. Vennell, S.W. Funke, S. Draper, C. Stevens, T. Divett, Designing large arrays of tidal turbines: a synthesis and review, Renew. Sustain. Energy Rev. 41 (2015) 454–472, 2015/01/01/.
[24] S.W. Funke, P.E. Farrell, M.D. Piggott, Tidal turbine array optimisation using the adjoint approach, Renew. Energy 63 (2014) 658–673, 2014/03/01/.
[25] L.E.M. Tim Daly, AbuBakr S. Bahaj, Experimental investigation of the effects of the presence and operation of tidal turbine arrays in A split tidal channel, in: Presented at the World Renewable Energy Congress - Sweden; 8-13 May; 2011, Linköping, Sweden, Sweden, 2011, https://doi.org/10.3384/ecp110574169. Abstract and Fulltext. Available:.
[26] M.G. Gebreslassie, G.R. Tabor, M.R. Belmont, Investigation of the performance of a staggered configuration of tidal turbines using CFD, Renew. Energy 80 (2015) 690–698, 2015/08/01/.
[27] M.J. Churchfield, Y. Li, P.J. Moriarty, A large-eddy simulation study of wake propagation and power production in an array of tidal-current turbines, Phil. Trans. Math. Phys. Eng. Sci. 371 (1985) (2013), 20120421, 2013/02/28.
[28] Y. Yuan, J. Tang, On advanced control methods toward power capture and load mitigation in wind turbines, Engineering 3 (4) (2017) 494–503, 2017/08/01/.
[29] Scott B. Capps, Charles S. Zender, Estimated global ocean wind power potential from QuikSCAT observations, accounting for turbine characteristics and siting, J. Geophys. Res. Atmos. 115 (D9) (2010).
[30] R. Vennell, An optimal tuning strategy for tidal turbines, in: eng (Ed.), Proc. Math. Phys. Eng. Sci. 472 (2195) (Nov 2016), 20160047.
[31] J. Bartl, L. Sætran, Experimental testing of axial induction based control strategies for wake control and wind farm optimization, J. Phys. Conf. 753 (2016), 032035, 09/01.
[32] M. Soleimanzadeh, R. Wisniewski, Controller design for a wind farm, considering both power and load aspects, Mechatronics 21 (4) (2011) 720–727, 2011/06/01/.
[33] M.C. Sousounis, J.K.H. Shek, M.A. Mueller, Modelling and control of tidal energy conversion systems with long distance converters, in: 7th IET International Conference on Power Electronics, Machines and Drives, PEMD 2014), 2014, pp. 1–6.
[34] M.C. Sousounis, J.K.H. Shek, Mitigation of Torque Pulsations in Variable Pitch Tidal Current Turbines Using Speed Control, 2017, https://doi.org/10.13140/RG.2.2.32130.17603.
[35] B. Sellar, Duncan R.J. Sutherland, Tidal energy site characterisation at the fall of warness, EMEC, UK, in: ENERGY TECHNOLOGIES INSTITUTE REDAPT MA1001 (MD3.8), Institute for Energy Systems, School of Engineering, University of EdinburghDecember, 2016. Available: http://redapt.eng.ed.ac.uk/library/eti/reports_updated/Technical%20Report%20on%20Tidal%20Site%20Characaterisation%20During%20the%20ReDAPT%20Project%20v4.0.pdf.
[36] National Renewable Energy Laboratory (05/05), Wind data and tools, Available: https://www.nrel.gov/wind/data-tools.html.
[37] L. Chen, P. Bonar, C. Vogel, T. Adcock, A note on the tuning of tidal turbines in channels, J. Ocean Eng. Marine Energy (2019), 03/11.
[38] D. Hunsaker, W. Phillips, Momentum Theory with Slipstream Rotation Applied to Wind Turbines, 2013.
[39] F.D. Bianchi, de Battista, Hernan, Ricardo J. Mantz, Wind Turbine Control Systems: Principles, Modelling and Gain Scheduling Design, Springer-Verlag, London, 2007.
[40] G.A. Hamill, J.A. McGarvey, D.A.B. Hughes, Determination of the efflux velocity from a ship's propeller, Proc. Instit. Civil Eng. - Maritime Eng. 157 (2) (2004) 83–91.
[41] W.-H. Lam, L. Chen, Equations used to predict the velocity distribution within a wake from a horizontal-axis tidal-current turbine, Ocean Eng. 79 (2014) 35–42, 2014/03/15/.
[42] A. Creech, A. Borthwick, D. Ingram, Effects of support structures in an LES actuator line model of a tidal turbine with contra-rotating rotors, Article vol, Energies 2017 (10) (2017), 5/19.
[43] Y. Zhang, Grid-connected Tidal Current Turbine Arrays - Electrical Modelling and Simulation, Mater of Science MSc thesis, School of Engineering, The University of Edinburgh, Edinburgh, 2018.
[44] D.C. Saunders, Wind Turbine Wake Interactions - Characterization of Unsteady Blade Forces and the Role of Wake Interactions in Power Variability Control, University of Vermont, 2017. PhD.
[45] S. Mbabazi, Investigating into Power Distribution/grid Interfacing for Subsea Tidal Generation - Rectification to a Common DC-bus, Doctor of Philosophy PhD Thesis, Department of Electrical and Electronics Engineering, The University of Sheffield, Sheffield, 2015.
[46] May 2015 Marine energy electrical architecture report 3: optimum electrical array architectures, Available: https://ore.catapult.org.uk/wp-content/uploads/2018/01/Marine-Energy-Electrical-Architecture-Report-3-Optimum-Electrical-Arra y-Architectures.pdf.
[47] B.G. Sellar, G. Wakelam, D.R.J. Sutherland, D.M. Ingram, V. Venugopal, Characterisation of tidal flows at the European marine energy centre in the absence of ocean waves, Energies 11 (1) (2018) 176.
[48] S. Brian, H. Samuel, R. Marshall, High-resolution velocimetry in energetic tidal currents using a convergent-beam acoustic Doppler profiler, Meas. Sci. Technol. 26 (8) (2015), 085801.
[49] R. Lam, S.L. Dubon, B. Sellar, C. Vogel, T. Davey, J. Steynor, Temporal and spatial characterisation of tidal blade load variation for structural fatigue testing, Renew. Energy 208 (2023/05/01/2023) 665–678.